International Journal of Applied Pharmaceutics

ISSN- 0975-7058 Vol 17, Issue 1, 2025

Original Article

EXPLORING NEW MONO AMINO OXIDASE-A (MAO-A) SELECTIVE INHIBITORS FROM CUCURBITO PEPO: A VIRTUAL SCREENING, MOLECULAR DOCKING, MD SIMULATIONS AND ADMET ANALYSIS

MAHENDRA GOWDRU SRINIVASA[1], SUDEEP D GHATE[2], R. SHYAMA PRASAD RAO[2], MANOHAR MAHADEV[3]*

[1]Nitte (Deemed to be University), NGSM Institute of Pharmaceutical Sciences (NGSMIPS), Department of Pharmaceutical Chemistry, Mangalore-575018, Karnataka, India. [2]Nitte (Deemed to be University), Center for Bioinformatics, Mangaluru-575018, Karnataka, India. [3]Nitte (Deemed to be University), NGSM Institute of Pharmaceutical Sciences (NGSMIPS), Department of Pharmaceutics Mangalore-575018, Karnataka, India

***Corresponding author: Manohar Mahadev; *Email: manohar.m@nitte.edu.in**

Received: 20 Jul 2024, Revised and Accepted: 26 Oct 2024

ABSTRACT

Objective: This study aimed to identify potential Monoamine oxidase (MAO) inhibitors from *Cucurbita pepo* to address the increasing prevalence of neurological and neuropsychiatric disorders, such as stroke, Alzheimer's, Parkinson's, autism, migraines, and depression, by targeting key enzymes involved in neurotransmitter degradation.

Methods: The study utilised molecular docking and pharmacological, physiological, and ADMET property analyses to screen compounds from *Cucurbita pepo*. Ten promising MAO inhibitors were shortlisted for further analysis. Extensive Molecular Dynamics (MD) simulations were conducted over 100 nanoseconds to assess the stability and dynamic behaviour within the MAO-A complex.

Results: Based on molecular docking results, four shortlisted compounds were identified as potential MAO-A inhibitors. Atomic-level docking studies were used to explore the binding mechanisms of the phytoconstituents within the active site of the MAO-A enzyme. The binding free energies of these compounds ranged from-9.183 to-6.001 kcal/mol. Phytoconstituent Compound C1 had the highest binding affinity with a G score of-9.183 kcal/mol, followed by Compound C2 with a G score of-9.045 kcal/mol. MD simulations further confirmed that both C1 and C2 formed highly stable complexes with MAO-A, suggesting their potential as effective inhibitors.

Conclusion: Compounds C1 and C2 from *Cucurbita pepo* show promise as stable and effective MAO-A inhibitors. Further experimental validation is required to confirm these findings and evaluate their therapeutic potential in treating neurological disorders.

Keywords: Antidepressant, *Curcubito pepo,* Docking, MAO-A

DOI: https://dx.doi.org/10.22159/ijap.2025v17i1.52084 Journal homepage: https://innovareacademics.in/journals/index.php/ijap

INTRODUCTION

In recent times, mental and behavioural disorders have emerged as essential contributors to disability due to their profound effects on the emotional well-being of individuals [1, 2]. According to a 2017 report from The global burden of disease, injuries, and Risk Factors Study, neuropsychiatric disorders have now risen to become the third leading cause of disability worldwide, with a higher prevalence among females [3, 4]. Moreover, the World Health Organization (WHO) has designated depressive disorders as a primary driver of non-fatal health burden on a global scale. In contrast, anxiety disorders hold the sixth position in this regard [5, 6]. Within this spectrum, depression stands out as the most prevalent condition, causing substantial suffering, and its occurrence is projected to increase considerably in the forthcoming years [7].

Specifically, depression is a catalyst for various physical ailments, including heart disease, kidney failure, stroke, diabetes, and cancer. Tragically, it can erode the will to live, pushing specific individuals towards contemplating suicide. Additionally, depression has even been identified as an early-stage precursor to Parkinson's Disease (PD). Stress, a widespread concern, often functions as a critical trigger for several diseases affecting the central nervous system.

Contemporary classes of antidepressants, such as selective serotonin reuptake inhibitors (SSRIs) (fig. 1) and Serotonin-Norepinephrine Reuptake Inhibitors (SNRIs) [8], have gained popularity due to their comparatively improved safety profiles and fewer dietary restrictions in contrast to older medications like Monoamine Oxidase Inhibitors (MAOIs) such as Isocarboxazid, Phenelzine, Selegiline, and Tranylcypromine (fig. 1) [9, 10]. These medications focus on extending the presence of neurotransmitters within synapses between nerve cells, thereby enhancing mood regulation. MAO enzymes have a pivotal role in the central nervous system by oxidatively deaminating and breaking down various amines/neurotransmitters like dopamine, serotonin, and norepinephrine, and thus play crucial roles in mood regulation, arousal, emotions, and even impulse control. These MAO enzymes are categorised into two types (MAO-A and MAO-B) [11]. MAO-A primarily influences serotonin, melatonin, and norepinephrine, while MAO-B is more associated with phenylethylamine and benzylamine.

However, both types can impact dopamine and tyramine. Clinically, inhibitors targeting MAO-A are utilised as antidepressants and anxiolytics, whereas MAO-B inhibitors find application in treating Parkinson's disease and the symptoms associated with Alzheimer's disease. Unfortunately, the utilisation of MAOIs in treating central nervous system disorders is limited due to side effects, notably hypertension triggered by the 'cheese effect' observed with irreversible and non-selective MAOIs [13].

Further, the current medications have adverse effects, including weight gain, sleep disturbances, and potential cardiovascular issues [14]. The pursuit of fresh alternatives for managing depression is prompting pharmacologists to explore diverse natural sources, particularly phytochemicals. Historically, numerous plants have been employed in addressing neurological health issues, with *Cucurbito pepo* (commonly known as pumpkin or squash, plant family Cucurbitaceae) standing out as an essential plant [14, 15]. The current research involves an *in silico* exploration of MAO-A inhibitors derived from *Cucurbito pepo* [16, 17].

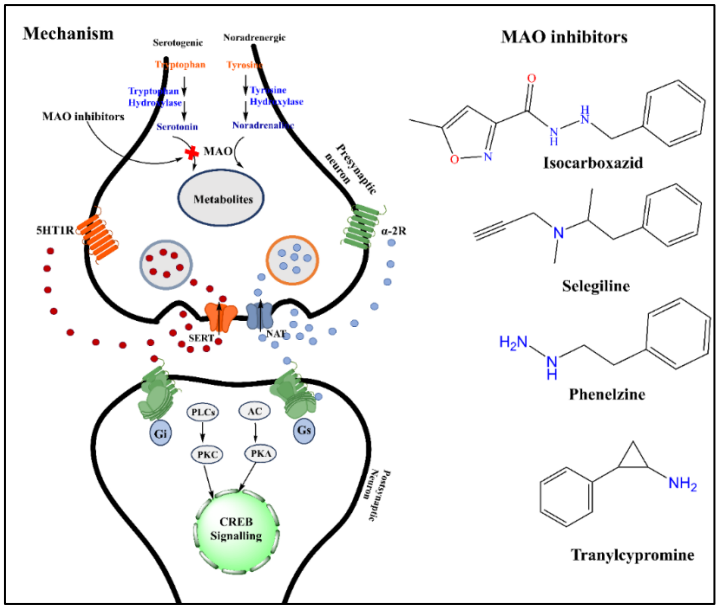

Fig. 1: The mechanism of action of monoamine oxidase inhibitors A and the structure of standard MAO enzyme inhibitors [12]

MATERIALS AND METHODS

Various components of the plant, such as its seeds, flesh, and even its flowers, have been harnessed for their prospective therapeutic attributes within traditional medicine/healing customs across the globe [16, 17].

Cucurbita pepo compounds

The candidate compounds from Cucurbita pepo were obtained from the IMPPAT database, Pubchem, and literature.

Bioinformatics tools

IMPPAT database (https://cb.imsc.res.in/imppat) [18, 19], ChemDraw version-20.1.1(https://informatics-support.perkinelmer.com), UCSF Chimera 1.8.1, PubChem (www.pubchem.com), RCSB PDB (http://www.rscb.org/pdb), Schrodinger software (https://www.schrodinger.com), SwissADME (http://www.swissadme.ch), Protox ii(https://tox-new.charite.de/protox_II) used in the present investigation.

Docking studies

Docking investigations were conducted using the Glide module within the Schrödinger 2020-3 suite, specifically the Maestro platform (https://www.schrodinger.com). These analyses were carried out on a Linux workstation.

Ligand preparation

Canonical SMILES representations of the 49 constituents from Curcubita pepo were sourced from PubChem and IMMPAT (https://cb.imsc.res.in/imppat). The top 10 compounds with the most favourable docking scores in their 2D structures, depicted in fig. 2, were singled out for subsequent investigation. These selected compounds underwent further processing using the LigPrep module of the Schrödinger suite (https://www.schrodinger.com). High-energy ionisation and tautomers were omitted to maintain consistent biological relevance during the Epik tool preparation phase. The highest-scoring ligands are presented in fig. 3. The prioritised ligands were assessed using Lipinski's rule of five via the Qikprop module to predict their potential properties [20].

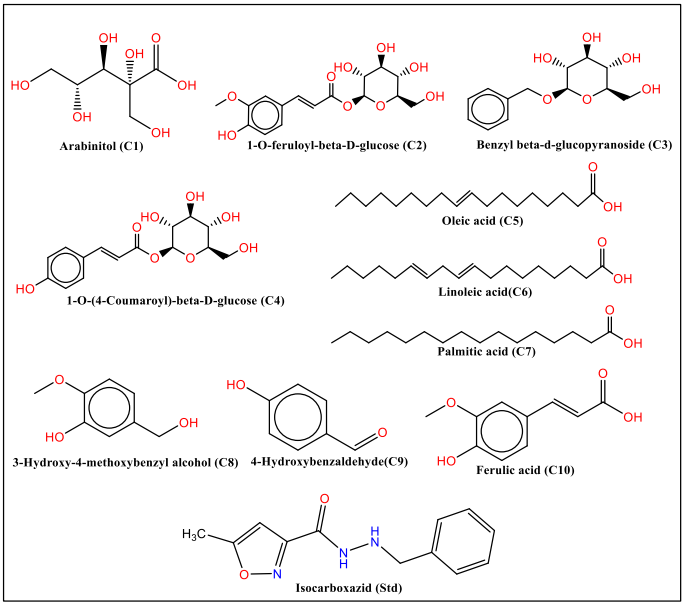

Fig. 2: Lead phytoconstituents of *Cucurbito pepo* and standard isocarboxazid

Protein preparation

The protein underwent preparation using the preparation wizard tool. The three-dimensional structure of the glucoamylase enzyme was acquired from the RCSB Protein Data Bank (https://www.rcsb.org). Specifically, the Crystal Structure of Human Monoamine oxidase-A with PDB ID: 2Z5Y [21] was utilised, having a resolution of 2.17 Å. The preparation involved adding missing hydrogen atoms, assigning proper bonding configurations, addressing potential metal interactions, and eliminating water molecules within 5 Å of heterogeneous groups. Hydrogen bonds were optimised through sample orientation, and all polar group hydrogen atoms were visible. Subsequently, the protein structure was minimised to its default root mean square deviation value of 0.30 Å [22, 23].

Protein-ligand docking

The receptor grid delineates the specific area within the target protein where the molecular docking process involves exploring ligand interactions. This grid was generated through the receptor grid generation interface within the Maestro Glide tool. The grid setup utilised the OPLS3e force field. The receptor folders were defined using LigPrep and then chosen for docking with the flexibility set to extra precision (XP) mode using the Glide module. The resultant binding interactions were ranked based on computed scores comprising the grid score, proprietary Glide score, and internal energy strain. These findings were visualised through the pose-viewer in various structural output formats. The Glide score was employed to predict binding affinity and prioritise ligands. The molecular docking study was conducted in the MAO-A inhibitors' docking program's extra precision (XP) mode.

Free energy calculation (-ΔG) by using prime/MMGBSA approach

The application of Schrödinger 2020-4 Prime molecular mechanics-generalized born surface area (MM-GBSA) was employed to compute the binding free energy of a protein-ligand complex. Additionally, post-docking energy minimisation studies were performed to deepen the analysis of the complex. The minimised docking pose of the protein-ligand complex, achieved through the extra precision (XP) docking process, underwent assessment using the OPLS3e force field and the Generalised-Born Surface Area (GBSA) continuum VSGB 2.0 solvent mode [24, 25].

Molecular dynamics simulations

The GROMACS (version 2021.6) (https://www.gromacs.org/) was employed to conduct MD simulations[24]. The initial stage encompassed the preparation of the complex by removing any heteroatoms. The CHARMM36 all-atom force field (version Feb 2021) was utilised for the protein topology, facilitated by GROMACS' pdb2 gmx module. The ligand topology was generated with the CHARMM General Force Field (CGenFF) server (https://cgenff.umaryland.edu/) and hydrogen addition. The point water model was used, and the simulation system was solvated in a dodecahedron box with 1 nm dimensions on all sides. Topreserve neutrality, necessary positive (Na^+) and negative (Cl^-) counter ions were introduced. Energy minimisation of the system utilised the steepest descent integrator, along with a Verlet cutoff scheme, for up to 50,000 steps. Subsequently, restraints were applied. Equilibration of the system occurred under canonical (NVT) and isobaric (NPT) ensembles for 1 ns, employing two coupling groups: protein-ligand and water-ions. Temperature control at 300 K employed the modified Berendsen thermostat (V-rescale), while the C-rescale pressure coupling algorithm maintained pressure at 1 bar. Long-range electrostatics, Coulombic interactions, and van der Waals forces were computed through the Particle Mesh Ewald (PME) method using a 1.2 nm cutoff. The LINCS algorithm constrained bond lengths. Each complex underwent a 100 ns MD simulation, during which coordinates and energies were saved every 20 picoseconds, resulting in 10,000 frames. The generated trajectories were analysed using built-in GROMACS utilities. Essential parameters, including Root mean Square Deviation (RMSD), Root mean Square Fluctuation (RMSF), Radius of Gyration (RoG), Solvent Accessible Surface Area (SASA), and hydrogen bond count, were computed across the 100 ns simulation duration. The outcomes were visualised using QtGrace [27, 28].

ADMET prediction

Pharmacokinetic properties encompassing absorption, distribution, metabolism, excretion parameters, and bioavailability of Phytoconstituents were assessed utilising the Swiss ADME online web tool (http://www.swissadme.ch/h)[29]. All selected ligands' different SMILES were employed as input files. Drug absorption hinges on factors such as being a P-glycoprotein substrate (P-gp substrate), water solubility, skin permeability (log Kp) levels, membrane permeability, and Gastrointestinal absorption (GSI). Notably, the blood-brain barrier (BBB) significantly influences drug distribution. Various CYP models facilitate assessing metabolism and volume of distribution, including types like CYP2C19 inhibitors, CYP1A2 inhibitors, and CYP3A4 inhibitors. Excretion primarily relies on total clearance, particularly of renal OCT2 substrate. For *in silico* toxicity prediction of proposed phytoconstituents, the freely accessible web server ProTox-II was utilised (http://tox.charite.de/protox-II) [29].

RESULTS AND DISCUSSION

Cucurbito pepo, belonging to the Cucurbita genus, is a cultivated plant encompassing various gourd and squash varieties. The seeds and pulp of C. pepo have traditionally been employed to address urinary tract issues, alleviate gastritis, and eliminate roundworms and tapeworms from the intestines. Pumpkin, a squash resembling a gourd within the Cucurbita genus and the Cucurbitaceae family, exhibits notable properties such as potent antioxidative, anti-depressive, and antihelminthic effects and antimicrobial activity. Studies on depression-induced rats have shown that alcoholic and aqueous extracts of C. pepo possess significant antioxidant and anti-depression attributes. Consequently, C. pepo may serve as a promising natural psychotherapeutic resource for combating depression [30].

Lipinski's rule

The leading bioactive phytoconstituents adhere to Lipinski's rule of five. Occasional violations of the Lipinski rule RO5 are deemed permissible, as illustrated in table 1. Consequently, the adherence of all the key phytoconstituents to this rule was evaluated, and each phytoconstituent was found to comply with Lipinski's RO5. Predicting in silico physicochemical attributes was employed to evaluate the compound's suitability for drug-like properties.

Table 1: Lipinski rule of 5 and drug-likeness score of bioactive phytoconstituents

Code	MW	Log p	Donor HB	Accept HB	Rule of Five
Acceptable range	≤500	>5	≤5	≤10	<5
C1	196.157	-1.246	4	7.55	1
C2	356.329	-0.781	5	12	0
C3	270.282	-0.383	4	10.2	0
C4	326.302	-0.854	5	11.25	0
C5	282.465	5.877	1	2	1
C6	280.45	5.827	1	2	1
C7	256.428	5.219	1	2	1
C8	154.165	0.712	2	3.2	0
C9	122.123	1.345	1	2.75	0
C10	194.187	1.356	2	3.5	0
Isocarboxazid	231.254	1.650	2	5	0

MW-Molecular weight; Log p–lipophilicity; Donor HB-Estimated number of donor hydrogen bonds; Accept HB-Estimated number of acceptor hydrogen bonds.

Docking studies

Table 2 displays the Glide scores representing the affinity of phytoconstituents for MAO-A (PDB ID: 2Z5Y) [31]. Docking studies at the atomic level were employed to decipher the binding mechanisms of all phytoconstituents within the active site of the MAO-A enzyme. The binding free energies of the phytoconstituents, ranging from-9.183 to-6.001 kcal/mol, are presented in table 2. The highest G score of-9.183 kcal/mol belongs to Phytoconstituent Compound C1, followed closely by Compound C2 with a G score of-9.045 kcal/mol. In Compound C1, hydrogen bonds form with Ile23, Gly49, Arg51, and Thr435, while Compound C2 establishes hydrogen bonds with Ala272 and Lys305. Noteworthy active residues within the chosen enzyme 2Z5Y encompass Gly22, Ile23, Ser24, Gly25, Gly50, Thr52, Val65, Gly66, Gly67, Ala68, Ala272, Ile273, Pro274, Val303, Phe352, Trp397, Cys406, Tyr407, Gly434, Thr435, Tyr444, Met445, and Ala448. The substantial affinity of these molecules is attributed to these interactions, as detailed in table 2. The most pronounced 2D interaction upon docking is illustrated in fig. 3. The standard Isocarboxazid exhibits fewer docking scores (-7.423 kcal/mol) when juxtaposed with the bioactive phytoconstituents. The 3D interactions of the top bioactive compounds with MAO-A are depicted in fig. 4 and 5 [32].

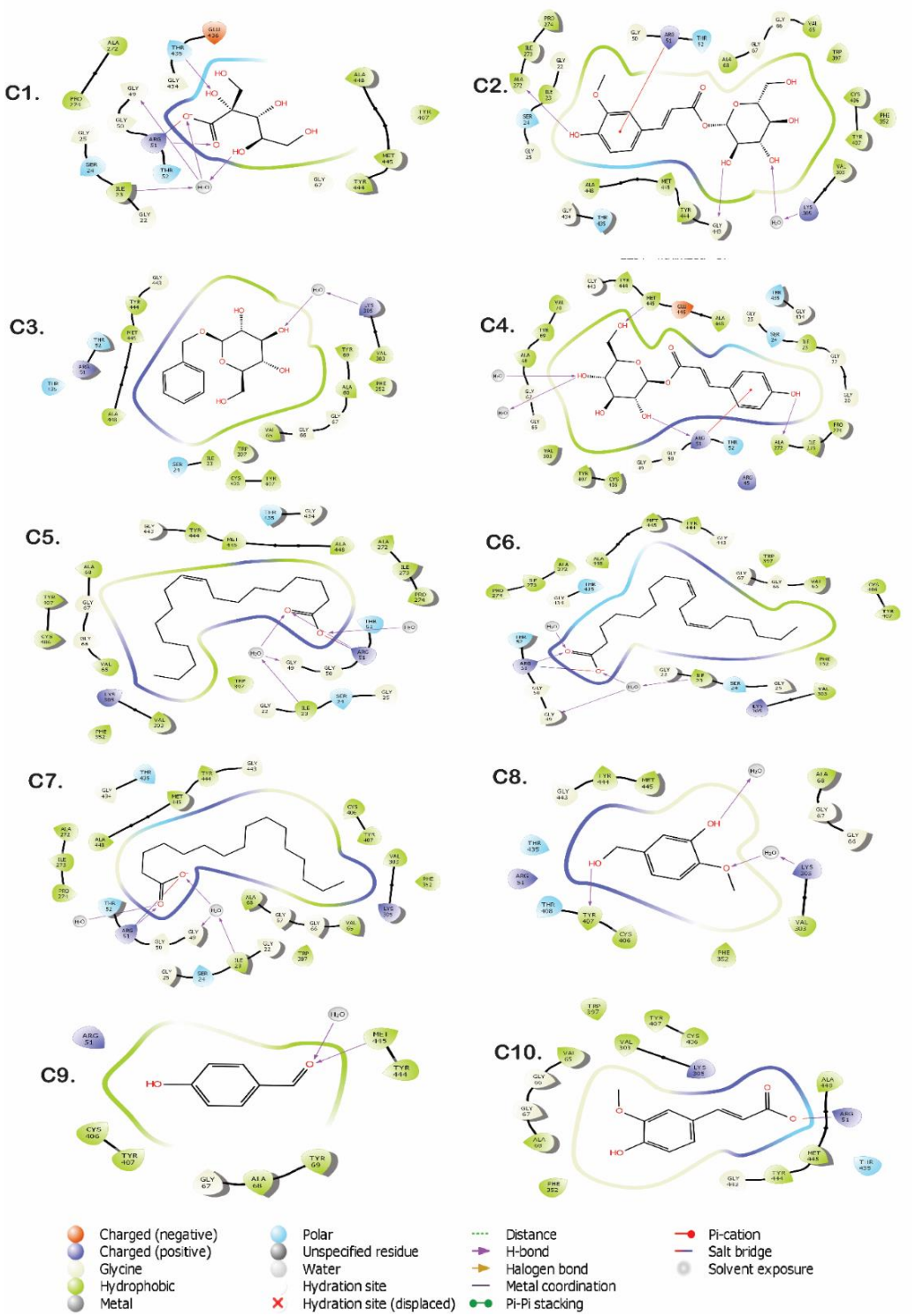

Fig. 3: 2D interaction of the top-ranked ligands with MAO-A

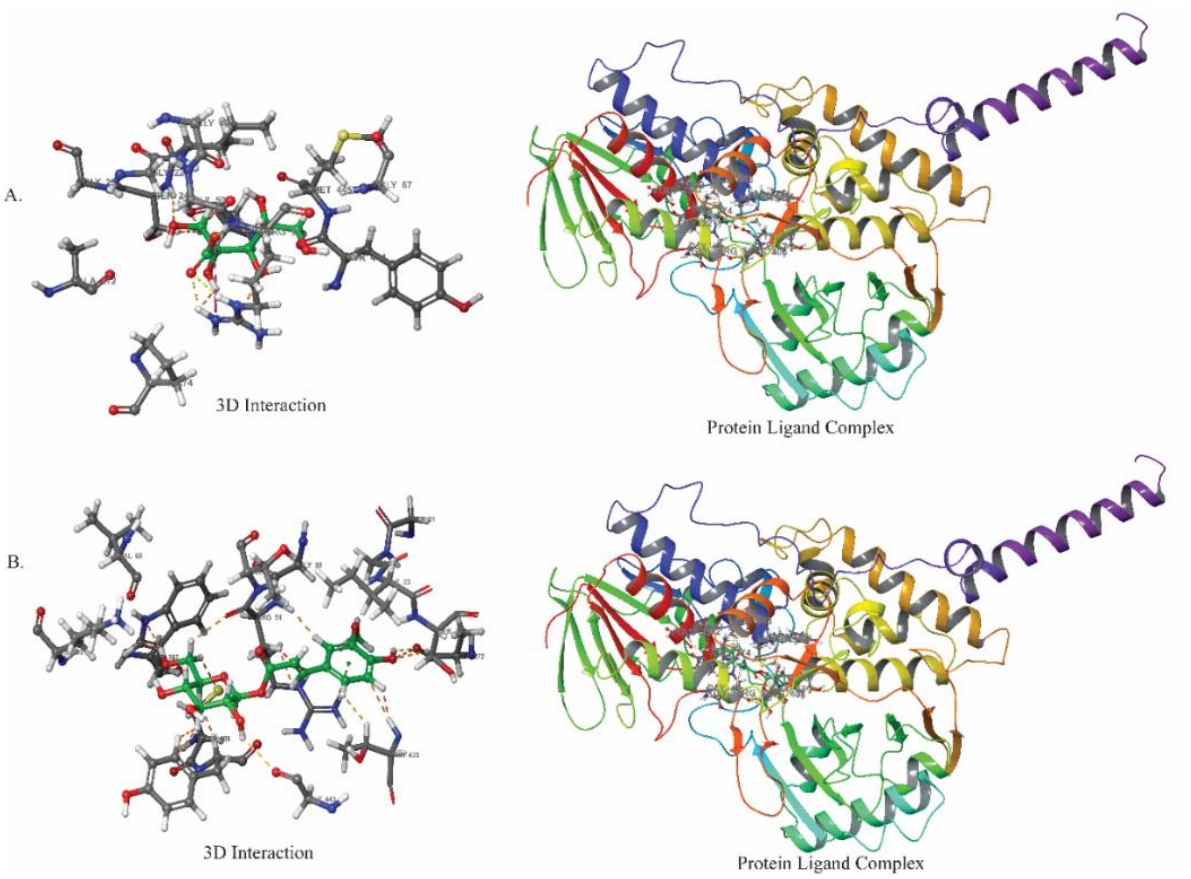

Fig. 4: A) 3D interaction of the ligands C1 with MAO-A, B) 3D interaction of the ligands C2 with MAO-A

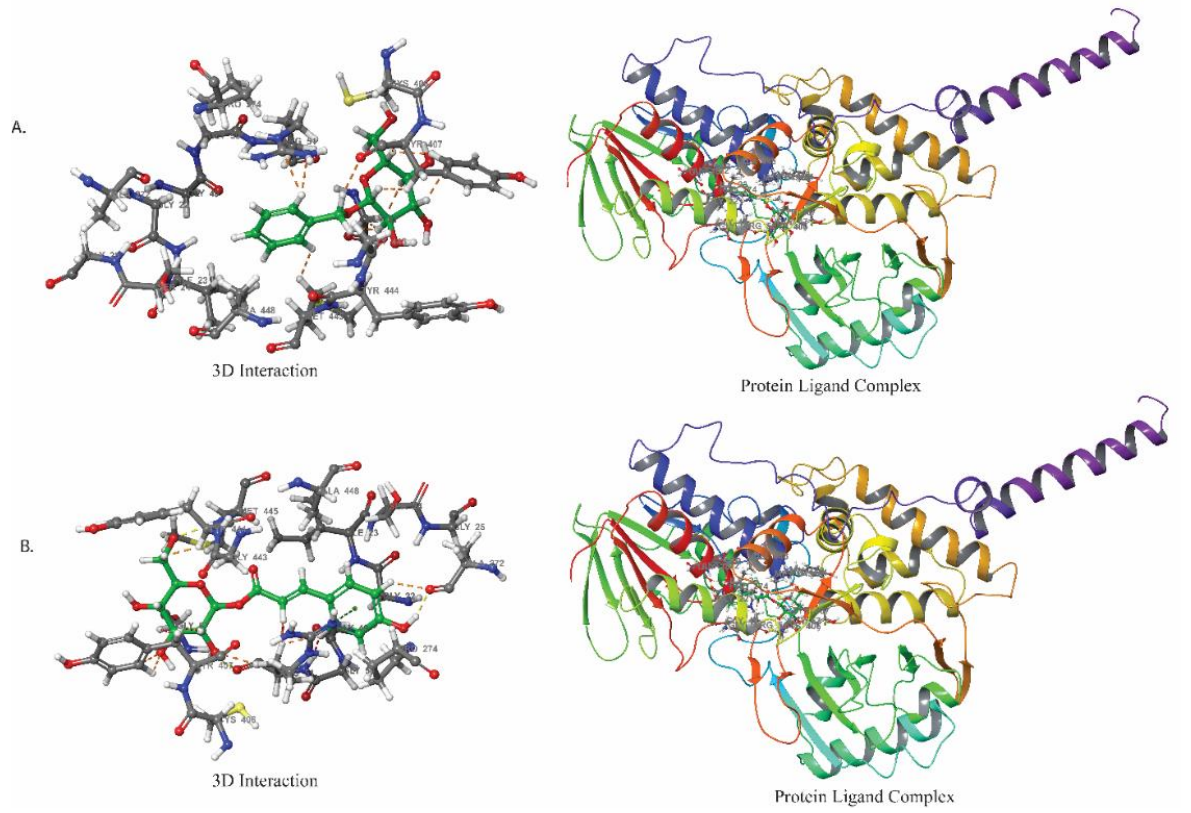

Fig. 5: A) 3D interaction of the ligands C3 with MAO-A, B) 3D interaction of the ligands C4 with MAO-A

Table 2: Interpretation of molecular docking of the *Cucurbita pepo* lead derivatives with control drug and their interactions with MAO protein (PDB ID: 2Z57)

CODE	Bioactive	Binding energy (kcal/mol)	H-bond residues	No of H-bond	Pi-cation	Salt bridge	Other bond residues
C1	Arabinitol	-9.183	Ile23, Gly49, Arg51, Thr435	4	-	Arg51	Gly22, Ser24, Gly25, Gly50, Thr52, Gly67, Ala272, Pro272, Tyr407, Gly434, Glu436, Tyr444, Met445, Ala448
C2	1-O-feruloyl-beta-D-glucose	-9.045	Ala272, Lys305, Gly443	3	Arg51	-	Gly22, Ile23, Ser24, Gly25, Gly50, Thr52, Val65, Gly66, Gly67, Ala68, Ala272, Ile273, Pro274, Val303, Phe352, Trp397, Cys406, Tyr407, Gly434, Thr435, Tyr444, Met445, Ala448
C3	Benzyl beta-d-glucopyranoside	-8.903	Lys305	1	-	-	Ile23, Ser24, Arg51, Thr52, Val65, Gly66, Gly67, Ala68, Tyr69, Val303, Phe352, Cyc406, Tyr407, Gly443, Tyr444, Met445, Ala448
C4	1-O-(4-oumaroyl)-beta-D-glucose	-8.774	Arg51, ala272, met445	3	-	Agr51	Gly20, Gly22, Ile23, Ser24, Gly25, Arg45, Gly49, Gly50, Thr52, Gly66, Gly67, Ala68, Tyr69, Val70, Ile273, Pro274, Val303, Cys406, Tyr407, Gly434, Thr435, Gly443, Tyr444, Met445, Glu446, Ala448
C5	Oleic acid	-7.893	Ile23, Gly49, Arg51	3	-	Arg51	Gly22, Ser24, Gly25, Gly50, Thr52, Val65, Gly66, Gly67, Ala68, Ala272, Ile273, Pro274, Val303, Lys305,
C6	Linoleic acid	-7.365	Ile23, Gly49, Arg51	3	-	Arg51	Gly22, Ser24, Gly25, Gly50, Thr52, Val65, Gly66, Gly67, Ala272, Ile273, Pro274, Val303, Lys305, Phe352, Cys406, Tyr407, Gly434, Thr435, Gly443, Tyr444, Met445, Ala448
C7	Palmitic acid	-7.284	Ile23, Gly49, Arg51	3	-	Arg51	Gly22, Ser24, Gly25, Gly50, Thr52, Val65, Gly66, Gly67, Ala272, Ile273, Pro274, Val303, Lys305, Phe352, Cys406, Tyr407, Gly434, Thr435, Gly443, Tyr444, Met445, Ala448
C8	3-Hydroxy-4-methoxybenzyl alcohol	-6.315	Lys305, Tyr407	2	-	-	Agr51, Gly66, Gly67, Ala68, Val303, Phe352, Cys406, Thr408, Thr435, Gly443, Tyr444, Met445
C9	4-Hydroxybenzaldehyde	-6.195	Met445	1	-	-	Arg51, Gly67, Ala68, Tyr69, Cys406, Tyr407, Tyr444
C10	Ferulic acid	-6.001	-	-	-	Arg51	Val65, Gly66, Gly67, Ala68, Val303, Lys305, Phe352, Trp397, Cys406, Tyr407, Thr435, Gly443, Tyr444, Met445, Ala448
Std	Isocarboxazid	-7.423	Lys305, Tyr407	2	-	-	Ile23, Ser24, Arg51, Thr52, Val65, Gly66, Gly67, Val303, Phe352, Trp397, Gly443, Tyr444, Met445, Ala448

Free energy calculation (-ΔG) using prime/MMGBSA approach

The study initially involves a docking simulation, which predicts how ligands fit into the enzyme's active site (catalytic pocket). Docking scores are numerical values that reflect the strength and quality of the interaction between the ligand and the enzyme. Higher (or more negative) docking scores typically indicate better binding affinity. After identifying ligands with favorable docking scores, a more detailed analysis is performed using Prime-MMGBSA. MMGBSA stands for Molecular Mechanics Generalized Born Surface Area, a method used to calculate the free binding energy (ΔG) of a ligand in complex with its target. Free energy (negative ΔG) measures how stable the ligand-enzyme complex is; more negative values suggest stronger and more stable binding. This method provides a more accurate evaluation compared to docking alone by considering various factors such as solvation effects and molecular flexibility. The compounds mentioned (C1, C4, C5, and C7) are chosen based on their elevated docking scores. Their free binding energies (ΔG) are then analyzed alongside the co-crystal ligand (the ligand already known to bind to MAO-A, used as a reference or control). The ligands show favorable stability within the catalytic pocket of MAO-A based on the combination of their docking scores and free binding energy values. This suggests that these compounds have a strong potential to bind effectively to MAO-A, which is important for their therapeutic potential.

The results of this analysis are summarized in a table (table 3), which likely presents the docking scores, free binding energy values, and possibly other relevant properties. These insights help researchers understand how these ligands interact with the target enzyme and their potential as MAO-A inhibitors, which could have implications for developing new therapies, especially in conditions where MAO-A is a key player (e. g., depression, neurodegenerative disorders) [33].

Table 3: Binding free energy calculation using prime/MM-GBSA approach

Bioactive	ΔGbind (Kcal/mol)	ΔGbind coulomb	ΔGbind covalent	ΔGbind vander	ΔGbind H Bond	ΔGbind lipophilic
C1	-93.02	-53.25	8.03	-42.23	-3.42	-60.11
C2	-63.20	-28.22	20.05	-47.60	-1.30	-43.16
C3	-60.83	-24.65	6.04	-29.30	-0.60	-37.31
C4	-72.78	-39.16	18.27	-45.97	-1.43	-40.17
C5	-84.37	-56.98	3.68	-32.84	-4.82	-61.58
C6	-72.67	-59.83	8.70	-25.47	-4.86	-63.32
C7	-97.58	-58.35	9.03	-46.92	-4.89	-65.02
C8	-50.79	-28.68	2.97	-24.86	-0.90	-18.20
C9	-32.93	-9.28	0.55	-23.13	-0.50	-10.69
C10	-34.75	-87.30	2.95	-37.55	-0.50	-24.11
Std	-52.05	-98.36	1.05	-31.43	-2.58	-23.24

The primary covalent interaction identified in C1 and C7 reduces the overall free-binding energy within the complex system. This interaction involves the creation of covalent bonds between the electrophilic functional group of the ligand and distinct nucleophilic amino acids situated within the protein's catalytic pocket. The decrease in energy is primarily attributed to a combination of electrostatic and hydrophobic interactions between the solute and the solvent, working together to enhance the stability of the complex. A comprehensive visual representation of the MM-GBSA model is depicted in fig. 6.

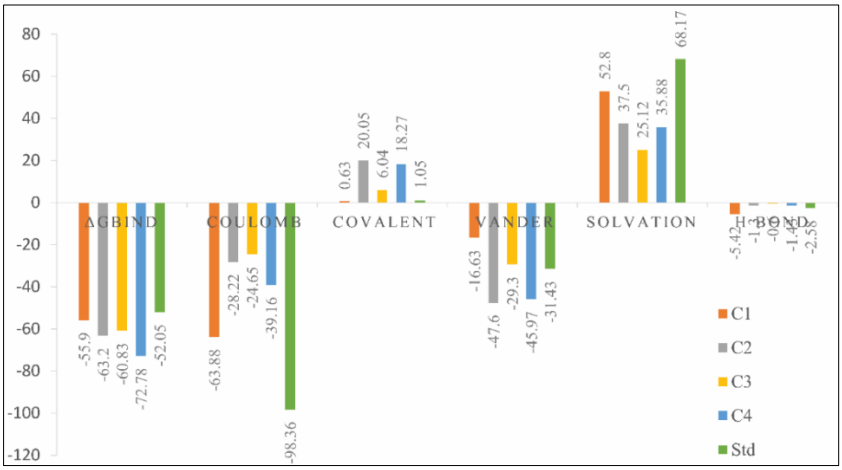

Fig. 6: The MM-GBSA method used to predict the complex's free binding energy (-ΔG)

This energy alteration arises from several factors, including Coulombic interactions (Coulomb), covalent bonding (Covalent), hydrogen bonding (H-bond), lipophilic interactions (Lipo), π-π packing interactions (Packing), the overall solvent effect, and van der Waals forces (VDW). Specific contributions are substantial among the factors influencing the negative Gibbs free energy (-ΔG). Notably, factors such as positively valued terms like covalent interactions and solvation energy have a notable impact, inducing instability within the complex system.

Molecular dynamics simulation (MDS) study

The study conducted a Molecular Dynamics Simulation (MDS) to explore the stability and dynamics of protein-ligand interactions, focusing on how the flexibility and stability of the protein-ligand complex change over time. The key elements of the analysis involved evaluating various structural parameters, including Root mean Square Deviation (RMSD), Root mean Square Fluctuation (RMSF), Radius of Gyration (Rg), hydrogen bond analysis, and Solvent Accessible Surface Area (SASA), all over a simulation duration of 100 ns (nanoseconds). Here's an elaboration of the key elements [34].

RMSD is used to track the stability of the protein-ligand complex by comparing the changes in the position of atoms (specifically the backbone atoms of the receptor) from the starting (crystal structure) to the final conformation. This parameter helps to determine whether the structure remains stable or undergoes significant conformational changes over the simulation time [35].

In this study, RMSD analysis was applied to two phytoconstituents, C1 and C2, in complex with the target protein (2Z5Y). The results showed minimal deviation for both complexes over the 100 ns period, suggesting that the complexes were highly stable. Notably, the C1-2Z5Y complex exhibited very consistent and stable conformations, with negligible fluctuations throughout the simulation, which implies that C1 interacts with the protein in a stable manner over time.

RMSF measures the flexibility of amino acid residues in the protein during the simulation. It tracks how much each residue deviates from its average position, indicating regions of the protein that are more flexible (high RMSF values) or more rigid (low RMSF values).

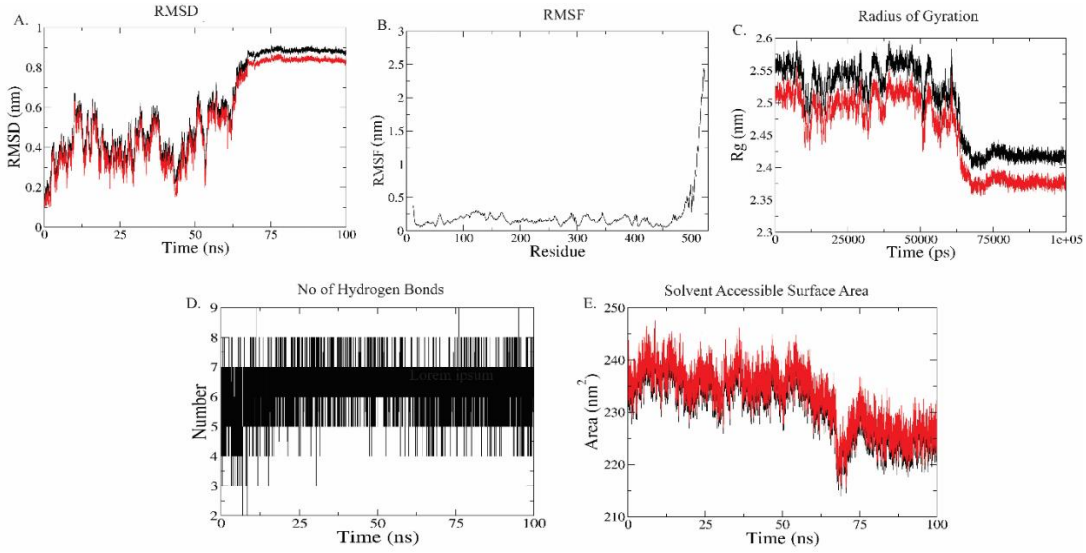

Fig. 7: Represents the stability of the complex (C1-2Z5Y) concerning (A) Root mean square deviation (RMSD) of the complex, (B) Root mean square fluctuation (RMSF) of the c-alpha atoms, (C) Radius of gyration (RoG) of the backbone (black) and complex (red), (D) Number of hydrogen bonds, (E) Solvent assessable surface area (SASA) for the protein(black) and complex (red)

For the complexes of C1 and C2, the RMSF values were analyzed to observe how ligand binding influences protein flexibility. Lower RMSF values indicated that the protein regions interacting with the ligands were more rigid, suggesting that the binding of the phytoconstituents stabilized those regions. This data provided insights into how the ligand affects the dynamic behavior of individual residues in the protein. Radius of Gyration (Rg) gives insight into the overall compactness or folding of the protein-ligand complex by measuring the distribution of the atoms relative to the central axis of the protein. It is used to monitor the changes in the protein's shape and structural compactness over the course of the simulation.

In this study, the Rg values for both the C1 and C2 complexes showed minimal deviations, indicating that the overall shape and folding of the protein remained stable throughout the 100 ns simulation. The Rg values remained in the range of ~0.05 nm, confirming that no significant unfolding or conformational collapse occurred during the interaction with the ligands. Hydrogen bonds are crucial for maintaining the stability of protein-ligand interactions. The formation and stability of hydrogen bonds between the protein and ligand provide insights into the strength of their interaction [36].

Analysis of Radius of Gyration (Rg) Consistency is evident in the radius of gyration (Rg) patterns, where masses calculated to root mean square distances are considered with the central axis of rotation. The Rg plot (fig. 7c and 8c) captures the shape, folding, and capability throughout the entire trajectory of the simulation. The native protein and the complex exhibit comparable Rg patterns over the simulation period, exhibiting minimal deviations within the range of ~0.05 nm.

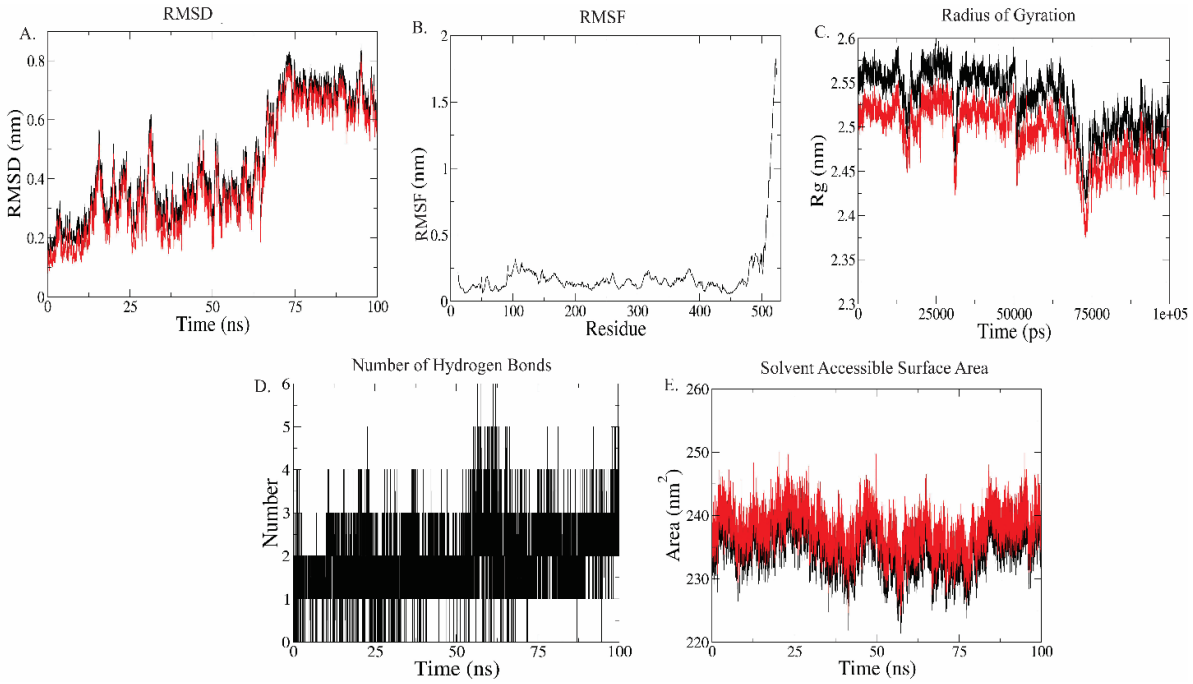

Fig. 8: Represents the stability of the complex (C2-2Z5Y) concerning (A) Root mean **Square Deviation (RMSD) of the complex, (B) Root** mean **Square Fluctuation (RMSF) of the c-alpha atoms, (C)Radius of Gyration (RoG) of the backbone (black) and complex (red), (D) Number of Hydrogen bonds (E) Solvent Assessable Surface Area (SASA) for the protein(black) and complex (red)**

To a certain extent, the stability assessment of the hydrogen bond analysis of the ligand-protein complex axes on intermolecular hydrogen bonds. The role of hydrogen bonds is paramount in scrutinising this complex. Hydrogen bond analysis, performed to characterise the stability of the C1-2Z5Y and C2-2Z5Y complexes, indicates a stronger affinity towards the target when four bonds are maximally formed at various time frames. Throughout the MDS, a consistent formation of 2 to 3 hydrogen bonds was maintained, signifying the stability of these chosen complexes, which collectively points to a robust ligand-target interaction, illustrated in fig. 7D and8D. Solvent Accessible Surface Area (SASA) Calculation: Structural integrity confirmation and the behaviour of biological macromolecules are influenced by solvent-accessible surface area (SASA). It is a criterion for evaluating the extent of receptor exposure to the surrounding solvent during MDS. However, ligand binding introduces structural changes in the protein, potentially altering the area in contact with the solvent. The SASA values of the protein plotted over time intervals track surface area changes (fig. 7E and 8E). For the C1-2Z5Y trajectory, values are reduced from 65 to 100 ns. Subsequently, slight fluctuations are evident during the simulation period. In the C2-2Z5Y complex, the trajectory demonstrates a stable value until around 100 ns. Overall, the SASA evaluation underscores the stable surface area of the protein within the complex during the simulation, as demonstrated in fig. 7E and 8E.

ADMET analysis

Predictions of pharmacokinetic and toxicological parameters for the chosen phytochemicals were conducted using the SwissADME server and Protox-ii. These server-based tools offer crucial insights such as molecular weight, general characteristics, polarity, hydrogen bond acceptor/donor count, lipophilicity, flexibility, water solubility, and pharmacokinetics (table 4). The molecular weights of the selected phytochemicals ranged from 154.165 to 356.36 g/mol (table 1). All molecules possessed fewer than 5 hydrogen bond acceptors and donors.

In the pharmacokinetics section table 4, diverse ADME characteristics of the investigated substances are evaluated using specialised models. The skin permeability coefficient (Kp) is predicted through a multiple linear regression model (MLR), which correlates with molecule size and lipophilicity (R2 = 0.67). Log Kp (cm/s) gauges a molecule's skin permeability, where a more negative Log Kp value indicates a lower skin permeation likelihood. Among the mentioned phytochemicals, C3 (-2.84 cm/s) demonstrates the least skin permeation, while C1 (-2.735 cm/s) displays high skin permeability. High skin permeability suggests suitability for transdermal treatments rather than oral medication.

Table 4: Predicted ADME parameters of the lead compounds

Property	Model	Unit	Compound			
			C1	C2	C3	C4
Absorption	Water solubility	(Log mol/l)	-2.702	2.408	-0.907	-1.81
	Caco2 permeability	(Log Papp in 10-6 cm/s)	-1.061	0.26	0.115	0.175
	Intestinal absorption (human)	(% Absorbed)	0	25.252	41.422	30.907
	Skin Permeability	(Log Kp)	-2.735	-2.787	-2.861	-2.846
	P-glycoprotein substrate	(Yes/No)	No	Yes	No	Yes
	P-glycoprotein I inhibitor	(Yes/No)	No	No	No	No
	P-glycoprotein II inhibitor	(Yes/No)	No	No	No	No
Distribution	VDss (human)	(Log L/kg)	-1.457	-1.457	-0.598	-0.601
	Fraction unbound (human)	(Fu)	0.536	0.536	0.56	0.552
	BBB permeability	(Log BB)	-1.806	-1.806	-0.868	-1.201
	CNS permeability	(Log PS)	-5.22	-5.22	-0.894	-3.908
Metabolism	CYP2D6 substrate	(Yes/No)	No	No	No	No
	CYP3A4 substrate	(Yes/No)	No	No	No	No
	CYP1A2 inhibitor	(Yes/No)	No	No	No	No
	CYP2C19 inhibitor	(Yes/No)	No	No	No	No
	CYP2C9 inhibitor	(Yes/No)	No	No	No	No
	CYP2D6 inhibitor	(Yes/No)	No	No	No	No
	CYP3A4 inhibitor	(Yes/No)	No	No	No	No
Excretion	Total Clearance	(Log ml/min/kg)	0.256	0.256	0.254	0.274
	Renal OCT2 substrate	(Yes/No)	No	No	No	No

Additionally, computer-based methods aid in assessing metabolomic attributes, particularly during early drug discovery stages. The studied phytochemicals exhibit high gastrointestinal absorption, some being blood-brain barrier permeants while others are non-BBB permeants (as detailed in table 4. Most of the investigated molecules satisfy drug-likeness criteria, except for P-glycoprotein binding. Additionally, bioactive total clearance and Renal OCT2 substrate data are presented in table 4. Toxicity analysis of the forty-nine selected phytoconstituents was performed using the Protox II online tool. The toxicity data unveiled that C1, C2, C3, and C4, particularly C2 and C4, exhibited immunotoxicity (table 5). Combining molecular docking and toxicity data, C1 and C3 emerged as the most promising drug molecules for managing MAO-A inhibitors. C1 belongs to class 6, while the rest are class 5 drugs with corresponding LD50 values (as presented in table 5). Comprehensive in silico toxicity parameters are outlined in table 5.

Table 5: Toxicity profile of leads bioactives from *Cucurbita pepo* using protox II

S. No.	Target feature	Compound-C1		Compound-C2		Compound-C3		Compound-C4	
		Prediction#		Prediction	Probability	Prediction	Probability	Prediction	Probability
1.	Hepatotoxicity	Inactive (0.95)	0.95	Inactive	0.82	Inactive	0.92	Inactive	0.83
2.	Carcinogenicity	Inactive	0.78	Inactive	0.81	Inactive	0.87	Inactive	0.79
3.	Immunotoxicity	Inactive	0.99	Active	0.99	Inactive	0.99	Active	0.66
4.	Mutagenicity	Inactive	0.82	Inactive	0.75	Inactive	0.83	Inactive	0.76
5.	Cytotoxicity	Inactive	0.80	Inactive	0.84	Inactive	0.87	Inactive	0.88
6.	Aryl hydrocarbon Receptor (AhR)	Inactive	0.99	Inactive	0.87	Inactive	0.96	Inactive	0.92
7.	Androgen Receptor (AR)	Inactive	1.0	Inactive	0.96	Inactive	0.55	Inactive	0.90
8.	Androgen Receptor Ligand Binding Domain (AR-LBD)	Inactive	0.99	Inactive	0.98	Inactive	0.60	Inactive	0.96
9.	Aromatase	Inactive	0.99	Inactive	0.98	Inactive	0.99	Inactive	0.98
10.	Estrogen Receptor Alpha (ER)	Inactive	0.99	Inactive	0.83	Inactive	0.61	Inactive	0.80
11.	Estrogen Receptor Ligand Binding Domain (ER-LBD)	Inactive	0.98	Inactive	0.96	Inactive	0.99	Inactive	0.96
12.	Peroxisome Proliferator-Activated Receptor Gamma (PPAR-Gamma)	Inactive	0.99	Inactive	0.97	Inactive	0.99	Inactive	0.97
13.	Nuclear factor (erythroid-derived 2)-like 2/antioxidant responsive element (nrf2/ARE)	Inactive	0.99	Inactive	0.96	Inactive	0.99	Inactive	0.97
14.	Heat shock factor response element (HSE)	Inactive	0.99	Inactive	0.96	Inactive	0.99	Inactive	0.97
15.	Mitochondrial Membrane Potential (MMP)	Inactive	0.99	Inactive	0.92	Inactive	0.97	Inactive	0.93
16.	Phosphoprotein (Tumor Suppressor) p53	Inactive	0.98	Inactive	0.88	Inactive	0.97	Inactive	0.88
17.	ATPase family AAA domain-containing protein 5 (ATAD5)	Inactive	0.99	Inactive	0.97	Inactive	0.99	Inactive	0.97
18.	Predicted LD50	7800 mg/kg		5000 mg/kg		4000 mg/kg		5000 mg/kg	
19.	Predicted Toxicity Class	6		5		5		5	
20.	Prediction accuracy	100%		69.26%		70.97%		69.26%	

#value in the brackets are probability

CONCLUSION

The present study delved into the urgent concern of mental and behavioural disorders, which have surged as significant contributors to global disability. The prevalence of neuropsychiatric disorders, particularly depression and anxiety, has escalated, leading to considerable suffering and worldwide disability. Traditional monoamine oxidase inhibitors (MAOIs), which target pivotal

neurotransmitters involved in mood regulation, have faced limitations due to their adverse effects. This research explored the potential antidepressant properties of phytochemicals sourced from natural origins, specifically on Cucurbita pepo. It unveiled noteworthy outcomes by conducting an extensive array of computational analyses. Molecular docking and dynamics simulations highlighted that the particular phytoconstituents, notably C1 and C2 derived from Cucurbita pepo, exhibited favourable interactions with the MAO-A enzyme, suggesting potential efficacy as antidepressants. These compounds showcased stability within the binding pocket and established essential hydrogen bonds with active site residues. Additionally, ADMET predictions emphasised the drug-like qualities of these compounds, showcasing favourable absorption, distribution, and metabolic characteristics. Toxicity analysis further indicated that C1 and C3 from Cucurbita pepo demonstrated promising safety profiles.

ACKNOWLEDGEMENT

We acknowledge the support from NGSM Institute of Pharmaceutical Sciences, Nitte (Deemed to be University), Mangalore, Karnataka, and NGSM-CADD Lab for providing all the necessary resources for this work.

FUNDING

Nil

AUTHORS CONTRIBUTIONS

MGS: conceptualisation, data analysis, and collection, writing the initial draft; SDG: data analysis, collection, and reviewing; SPR: reviewing and editing, checking of scientific accuracy. MM: conceptualisation, supervision, reviewing and editing.

CONFLICT OF INTERESTS

All the authors declare that they have no conflict of interest.

REFERENCES

1. Reed GM, First MB, Billieux J, Cloitre M, Briken P, Achab S. Emerging experience with selected new categories in the ICD-11: complex PTSD prolonged grief disorder gaming disorder and compulsive sexual behaviour disorder. World Psychiatry. 2022;21(2):189-213. doi: 10.1002/wps.20960, PMID 35524599.
2. Van Duinkerken E, Snoek FJ, DE Wit M. The cognitive and psychological effects of living with type 1 diabetes: a narrative review. Diabet Med. 2020;37(4):555-63. doi: 10.1111/dme.14216, PMID 31850538.
3. Deuschl G, Beghi E, Fazekas F, Varga T, Christoforidi KA, Sipido E. The burden of neurological diseases in Europe: an analysis for the global burden of disease study 2017. Lancet Public Health. 2020;5(10):e551-67. doi: 10.1016/S2468-2667(20)30190-0, PMID 33007212.
4. Luo Z, LV H, Chen Y, XU X, Liu K, LI X. Years of life lost due to premature death and their trends in people with selected neurological disorders in shanghai China 1995-2018: a population based study. Front Neurol. 2021;12:625042. doi: 10.3389/fneur.2021.625042, PMID 33746880.
5. DE Mendonca Lima CA, DE Leo D, Ivbijaro G, Svab I. Suicide prevention in older adults. Asia Pac Psychiatry. 2021;13(3):e12473. doi: 10.1111/appy.12473, PMID 34114355.
6. Tsirmpas C, Andrikopoulos D, Fatouros P, Eleftheriou G, Anguera JA, Kontoangelos K. Feasibility engagement and preliminary clinical outcomes of a digital biodata-driven intervention for anxiety and depression. Front Digit Health. 2022 Jul;4:868970. doi: 10.3389/fdgth.2022.868970, PMID 35958737.
7. Subba R, Sandhir R, Singh SP, Mallick BN, Mondal AC. Pathophysiology linking depression and type 2 diabetes: psychotherapy physical exercise and fecal microbiome transplantation as damage control. Eur J Neurosci. 2021;53(8):2870-900. doi: 10.1111/ejn.15136, PMID 33529409.
8. Jia E, Bartlett MG. Recent advances in liquid chromatographic methods for the determination of selective serotonin reuptake inhibitors and serotonin norepinephrine reuptake inhibitors. Biomed Chromatogr. 2020;34(3):e4760. doi: 10.1002/bmc.4760, PMID 31758582.
9. Tijani AO, Nunez E, Singh K, Khanna G, Puri A. Transdermal route: a viable option for systemic delivery of antidepressants. J Pharm Sci. 2021;110(9):3129-49. doi: 10.1016/j.xphs.2021.05.015, PMID 34089714.
10. Robertson L, Bertolini F, Meader N, Davies SJ, Barbui C, Gilbody S. Antidepressants for major depression disorder in older people: a network meta analysis. Cochrane Database Syst Rev. 2019 Sep 5;2019(9):CD013394. doi: 10.1002/14651858.CD013394.
11. Behl T, Kaur D, Sehgal A, Singh S, Sharma N, Zengin G. Role of monoamine oxidase activity in alzheimer's disease: an insight into the therapeutic potential of inhibitors. Molecules. 2021;26(12):1-21. doi: 10.3390/molecules26123724, PMID 34207264.
12. Baweja GS, Gupta S, Kumar B, Patel P, Asati V. Recent updates on structural insights of MAO-B inhibitors: a review on target based approach. Mol Divers. 2024;28(3):1823-45. doi: 10.1007/s11030-023-10634-6, PMID 36977955.
13. Chamberlain SR, Baldwin DS. Monoamine oxidase inhibitors (MAOIs) in psychiatric practice: how to use them safely and effectively. CNS Drugs. 2021;35(7):703-16. doi: 10.1007/s40263-021-00832-x, PMID 34240393.
14. Ferguson JM. SSRI antidepressant medications: adverse effects and tolerability. Prim Care Companion J Clin Psychiatry. 2001 Feb;3(1):22-7. doi: 10.4088/pcc.v03n0105, PMID 15014625.
15. Sinha S, Kumar B, Luqman S, Singh DK. Neuroprotective potential of cucurbita maxima duchesne ex poir caeselpenia bunduc (L.) roxb and bombax ceiba linn extracts. S Afr J Bot. 2019;120:319-25. doi: 10.1016/j.sajb.2018.09.027.
16. Heinrich M, Frei Haller B, Leonti M. A perspective on natural products research and ethnopharmacology in mexico: the eagle and the serpent on the prickly pear cactus. J Nat Prod. 2014;77(3):678-89. doi: 10.1021/np4009927, PMID 24559070.
17. Adnan M, Gul S, Batool S. A review on the ethnobotany phytochemistry pharmacology and nutritional composition of Cucurbita pepo L. J Phytopharm. 2017;6(2):133-9.
18. Shokrzadeh M, Azadbakht M, Ahangar N, Hashemi A, Saeedi Saravi SS. Cytotoxicity of hydro alcoholic extracts of Cucurbitapepo and Solanum nigrum on HepG2 and CT26 cancer cell lines. Pharmacogn Mag. 2010;6(23):176-9. doi: 10.4103/0973-1296.66931, PMID 20931075.
19. Vivek Ananth RP, Mohanraj K, Sahoo AK, Samal A. IMPPAT 2.0: an enhanced and expanded phytochemical atlas of Indian medicinal plants. ACS Omega. 2023;8(9):8827-45. doi: 10.1021/acsomega.3c00156, PMID 36910986.
20. Mohanraj K, Karthikeyan BS, Vivek Ananth RP, Chand RP, Aparna SR, Mangalapandi P. IMPPAT: a curated database of Indian medicinal plants phytochemistry and therapeutics. Sci Rep. 2018;8(1):4329. doi: 10.1038/s41598-018-22631-z, PMID 29531263.
21. Malkaje S, Srinivasa MG, Deshpande NS, Navada S, Revanasiddappa BC. An in silico approach: design homology modeling molecular docking MM/GBSA simulations and a dmet screening of novel 1,3,4-oxadiazoles as PLK1inhibitors. Curr Drug Res Rev. 2023;15(1):88-100. doi: 10.2174/2589977514666220821203739, PMID 36017854.
22. Moorkoth S, Prathyusha NS, Manandhar S, Xue Y, Sankhe R, Pai KS. Antidepressant like effect of dehydrozingerone from Zingiber officinale by elevating monoamines in brain: in silico and *in vivo* studies. Pharmacol Rep. 2021;73(5):1273-86. doi: 10.1007/s43440-021-00252-0, PMID 34181212.
23. Pirolli D, Righino B, DE Rosa MC. Targeting SARS-CoV-2 spike protein/ACE2 protein-protein interactions: a computational study. Mol Inform. 2021;40(6):e2060080. doi: 10.1002/minf.202060080, PMID 33904240.
24. Muddagoni N, Bathula R, Dasari M. Homology modelling virtual screening prime mmgbsa autodock identification of inhibitors of FGR protein. Biointerface Res Appl Chem. 2021;11(4):11088-103. doi: 10.33263/BRIAC114.1108811103.
25. Jayasurya BR, Swathy JS, Dinesh S, Sharma S. Molecular docking and investigation of Boswellia serrata phytocompound as cancer therapeutics to target growth factor receptors: an in silico approach. Int J Appl Pharm. 2023 Apr 21;15(4):173-83. doi: 10.22159/ijap.2023v15i4.47833.

26. Musfiroh I, Sigalingging OS, Suhandi C, Khairul Ikram NK, Megantara S, Muchtaridi M. In silico study of some flavonoid compounds against ace-2 receptors as anti-COVID-19. Int J App Pharm. 2023;15(4):225-30. doi: 10.22159/ijap.2023v15i4.48109.
27. Odhar HA, Hashim AF, Ahjel SW, Humadi SS. Virtual screening of FDA-approved drugs by molecular docking and dynamics simulation to recognise potential inhibitors against mycobacterium tuberculosis enoyl acyl carrier protein reductase enzyme. Int J Appl Pharm. 2024;16(1):261-6. doi: 10.22159/ijap.2024v16i1.49471.
28. Machado RR, Eitzinger J. Laukemann J. MD-Bench: engineering the in core performance of short-range molecular dynamics kernels from state of the art simulation packages. Chemical Physics. 2023;17. doi: 10.48550/arXiv.2302.14660.
29. Halder SK, Mim MM, Alif MM, Shathi JF, Alam N, Shil A. Oxa-376 and Oxa-530 variants of β-lactamase: computational study uncovers potential therapeutic targets of acinetobacter baumannii. RSC Adv. 2022;12(37):24319-38. doi: 10.1039/d2ra02939a, PMID 36128545.
30. Azzam KA. Swiss ADME and pk CSM webservers predictors: an integrated online platform for accurate and comprehensive predictions for in silico ADME/T properties of artemisinin and its derivatives. KIMS/CUMR/MShKP. 2023;325(2):14-21. doi: 10.31643/2023/6445.13.
31. Ghosh S, Tripathi P, Talukdar P. In silico study by using protox-II webserver for oral acute toxicity organ toxicity immunotoxicity genetic toxicity endpoints nuclear receptor signalling and stress response pathways of synthetic pyrethroids. World Sci News. 2019 Jun;132:35-51.
32. Larit F, Elokely KM, Chaurasiya ND, Benyahia S, Nael MA, Leon F. Inhibition of human monoamine oxidase A and B by flavonoids isolated from two algerian medicinal plants. Phytomedicine. 2018 Feb 1;40:27-36. doi: 10.1016/j.phymed.2017.12.032, PMID 29496172.
33. Huang C, Xiong J, Guan HD, Wang CH, Lei X, HU JF. Discovery synthesis biological evaluation and molecular docking study of (R)-5-methylmellein and its analogs as selective monoamine oxidase a inhibitors. Bioorg Med Chem. 2019 May 15;27(10):2027-40. doi: 10.1016/j.bmc.2019.03.060, PMID 30975503.
34. Mehta P, Srivastava S, Sharma M, Singh I, Malik R. Identification of chemically diverse GABAA agonists as potential anti-epileptic agents using structure guided virtual screening ADMET quantum mechanics and clinical validation through off target analysis. Int J Biol Macromol. 2018 Nov 1;119:1113-28. doi: 10.1016/j.ijbiomac.2018.08.032, PMID 30098361.
35. Liu K, Watanabe E, Kokubo H. Exploring the stability of ligand binding modes to proteins by molecular dynamics simulations. J Comput Aided Mol Des. 2017 Feb;31(2):201-11. doi: 10.1007/s10822-016-0005-2, PMID 28074360.
36. Mollaamin F, Layali I, Ilkhani AR, Monajjemi M. Nanomolecular simulation of the voltage-gated potassium channel protein by gyration radius study. Afr J Microbiol Res. 2010 Dec 18;4(24):2795-803.